Exciton magnetic polaron in semimagnetic semiconductor nanocrystals

A. K. Bhattacharjee
Laboratoire de Physique des Solides, URA au CNRS, Université Paris–Sud, 91405 Orsay, France

C. Benoit à la Guillaume
Groupe de Physique des Solides, URA au CNRS, Université Denis Diderot et Université Pierre et Marie Curie, 2 place Jussieu, 75251 Paris Cedex 05, France

(Received 20 May 1996; revised manuscript received 11 February 1997)

We present a theoretical study of the magnetic polaron associated with an electron-hole pair in a diluted magnetic semiconductor quantum dot. It is based on the effective-mass approximation in the strong confinement regime, which incorporates the coupling between the light- and heavy-hole bands. The magnetic polaron, arising from the sp-d exchange interaction between the confined carriers and the magnetic ions, is treated in a self-consistent mean-field approach that leads to coupled nonlinear Schrödinger equations for the electron and the hole. The local response to the effective field is modeled by the experimental high-field magnetization curve in the bulk. The electron-hole Coulomb interaction is taken into account. An exact numerical solution of the three coupled equations is used to calculate the equilibrium polaron size, binding energy (E_p), and spin (S_p). Results are first presented for $Cd_{1-x}Mn_xTe$ nanocrystals with $x=0.11$. E_p decreases and the orbital contraction increases with an increasing quantum dot radius (a). In small dots, approaching saturation in the core region, E_p decreases slowly as the temperature (T) increases. In large dots $E_p(T)$ decreases rapidly towards the fluctuation regime, where $E_p \propto a^{-3}$. A similar temperature dependence is obtained for S_p; the fluctuation-regime value is, however, size independent. The light-induced magnetization enhancement due to polaron formation is considered and an optimal quantum dot radius is predicted to be ~ 30 Å. We have also calculated E_p as a function of an applied magnetic field, which shows a decreasing behavior that depends on a and T. Theoretical results for $Cd_{1-x}Mn_xSe$ nanocrystals show a good agreement with recently reported experimental data on the photoluminescence Stokes shift *versus* magnetic field. [S0163-1829(97)02508-3]

I. INTRODUCTION

Semiconductor nanocrystallites, also called quantum dots (QD's), have been studied a lot in recent years.[1] In particular, high-quality nanocrystals of II-VI compounds have been fabricated and their optical properties investigated in great detail,[2] including well-characterized ''band-edge'' luminescence. The confinement-induced blueshift of the fundamental gap and the discretization of the energy spectrum have been observed. On the other hand, semimagnetic or diluted magnetic semiconductors (DMS) based on II-VI compounds, such as $Cd_{1-x}Mn_xTe$, are known for giant magneto-optical properties and magnetic polarons.[3] These effects arise from strong sp-d exchange interactions between the band carriers and the Mn^{2+} ions. Bound magnetic polarons associated with shallow impurities (donors and acceptors) have been extensively studied.[4] Localized exciton magnetic polarons have also been reported in bulk and in epilayer $Cd_{1-x}Mn_xTe$ (Ref. 5) and in $CdTe/Cd_{1-x}Mn_xTe$ heterostructures.[6] Acceptor-bound magnetic polarons approach the saturation regime at low temperature;[7–13] the mutual spin polarization between the bound hole and the Mn ions situated in its orbit tends to form a ferromagnetic cluster. A similar situation is expected in an optically excited small DMS nanocrystal with additional contribution from the electron. In fact, such a QD should be a model for a zero-dimensional exciton magnetic polaron, provided that the polaron formation time is shorter than the lifetime of the electron-hole pair.

Wang *et al.*[14] reported an experimental investigation on DMS nanocrystals. $Zn_{0.93}Mn_{0.07}S$ crystallites of average diameter $\simeq 25$ Å were grown in a glass matrix. The observed photoluminescence (PL) peak at 2.12 eV corresponds to the well-known Mn^{2+} internal emission. The PL-excitation spectrum yielded a quantum-confinement blueshift of 0.23 eV for the fundamental gap. They also measured the static magnetic susceptibility from 2.3 K to 314 K; the data fit the Curie-Weiss law with a negligibly small Θ value, suggesting a smaller contribution of antiferromagnetic Mn-Mn interaction in the QD than in the bulk. More recently, Bhargava *et al.*[15] studied coated Mn-doped ZnS particles of diameter varying from 35 to 75 Å; they focused on the characteristics of the Mn^{2+} luminescence. In fact, DMS materials such as $Zn_{1-x}Mn_xS$ with the bulk band gap well above 2.12 eV seem unsuitable for studying the magnetic polaron, as the PL spectrum is dominated by the Mn emission. This is because the time of energy transfer from an electron-hole pair to the Mn d shell is short (<500 psec),[15] perhaps in the range of the polaron formation time (~ 100 psec in the bulk).[5] In this respect, magneto-optical studies of $Cd_{1-x}Mn_xSe$ nanocrystals embedded in quartz glass, reported by Yanata *et al.*,[16] are more interesting; their exciton luminescence data do provide evidence for magnetic polaron. The PL Stokes shift under selective excitation was found to decrease in the presence of a magnetic field and to saturate in a field of 6 T. Such a behavior is typical of localized exciton magnetic polaron. Moreover, picosecond time-resolved spectroscopy indicated

a decrease of the QD exciton lifetime from 900 to 400 ps in a magnetic field of 5 T.

An early theoretical study of the magneto-optical properties of DMS nanocrystals was presented by one of us.[17] It was based on the effective-mass approximation in the strong confinement regime.[21,22] The confinement-induced mixing between the light- and heavy-hole states was found to yield a reduction of the Zeeman splitting of the fourfold hole ground state. An exactly soluble ''spin cluster'' model was used for calculating the equilibrium properties of the magnetic polaron associated with an electron-hole pair in the zinc-blende $Cd_{1-x}Mn_xTe$ quantum dot. The calculation was later[18] extended to the hexagonal case $Cd_{1-x}Mn_xSe$ and compared with the experimental data of Ref. 16. The reduced Zeeman shift fitted the magnetoabsorption data, while the field dependence of the polaron binding energy showed qualitative agreement with the PL Stokes shift data.

In this paper we present a more realistic model for the magnetic polaron (MP). It is based on a self-consistent mean-field approach previously applied to the cases of bound[19] and free[20] hole magnetic polarons. We first generalize the theory in order to incorporate the fourfold degeneracy of the unperturbed valence band. In the spherical approximation, assuming a $1S_{3/2}$ ground state for the confined hole, after averaging out the angular dependence of the sp-d exchange field, we deduce the effective-mass equations. These are three coupled nonlinear differential equations for the three radial envelope functions corresponding to the electron, and the s- and d-like parts of the hole. An experimental high-field magnetization curve is then used to modelize the response of the Mn spins to the local exchange field due to the electron and the hole. The direct Coulomb interaction between the carriers is also taken into account in the Hartree approximation. An exact numerical solution is used to calculate the equilibrium properties of the magnetic polaron. Results are first presented for QD's of $Cd_{1-x}Mn_xTe$ with $x=0.11$. The self-consistent contraction of the hole and electron radii is discussed. In addition to the characteristic decreasing behaviors of the polaron binding energy with increasing temperature or magnetic field, we find that the energy decreases with increasing QD radius. The temperature and size dependence of the spontaneous magnetic moment of the polaron is also investigated. The saturation regime is approached in small dots. The ratio of the superparamagnetic polaron magnetization to the paramagnetic QD magnetization in the low-field limit, which should be an indication of the light-induced magnetization enhancement, is studied. We thus estimate the optimum QD radius for this effect to be around 30 Å. Finally, the model is applied to the case of $Cd_{0.9}Mn_{0.1}Se$ nanocrystals; the calculated field dependence of the polaron binding energy shows a good agreement with the experimental photoluminescence Stokes shift data.[16]

II. THEORY

We consider a spherical QD of radius a smaller than the bulk exciton Bohr radius a_B; in this strong confinement regime, neglecting the small excitonic correlation, the lowest-energy state of an electron-hole (e-h) pair can be written as

$$\Psi^{e\text{-}h}_{m\mu}(\mathbf{r}_e,\mathbf{r}_h)=\psi^e_m(\mathbf{r}_e)\psi^h_\mu(\mathbf{r}_h). \tag{1}$$

Here the electron wave function is

$$\psi^e_m(\mathbf{r})=\phi(\mathbf{r})u^c_m(\mathbf{r}). \tag{2}$$

In a spherical potential the envelope function $\phi(\mathbf{r})$ is of the $1s$ type; the unperturbed version is given by[22]

$$\phi_0(\mathbf{r})=\sqrt{\frac{2}{a}}\frac{\sin(\pi r/a)}{r}Y_{00}. \tag{3}$$

$u^c_m(\mathbf{r})$ is the conduction band Bloch function at Γ, with $m=s_z=\pm\frac{1}{2}$. In the spherical approximation for the Luttinger Hamiltonian the hole wave functions are

$$\psi^h_\mu(\mathbf{r})=\sum_\nu F_{\nu\mu}(\mathbf{r})u^h_\nu(\mathbf{r}), \tag{4}$$

where μ, ν run through $\frac{3}{2}$, $\frac{1}{2}$, $-\frac{1}{2}$, and $-\frac{3}{2}$. $u^h_\nu(\mathbf{r})$ are the time-reversed valence band Bloch functions at Γ, with $j_z=\nu$. Note that, following Xia[21] and Efros,[22] we have included only the fourfold Γ_8 valence band in Eq. (4). Very recently, Richard *et al.*[23] have reported that the contribution from the spin-orbit split-off band Γ_7 might be of crucial importance for the QD hole level ordering. Here, we consider the dipole-active fourfold ground state $1S_{3/2}$ that corresponds to

$$F_{\nu\mu}(\mathbf{r})=\delta_{\nu\mu}R_0(r)Y_{00}+\langle\tfrac{3}{2},\nu;2,(\mu-\nu)|\tfrac{3}{2},\mu\rangle \times R_2(r)Y_{2,\mu-\nu}(\theta,\varphi), \tag{5}$$

where Clebsch-Gordan coefficients have been used. The above functional forms remain valid in any potential of spherical symmetry.[24] So, we can use them as long as the effective exchange field retains this symmetry. The unperturbed QD functions $R_0(r)$ and $R_2(r)$ can be written in terms of the spherical Bessel functions.[22]

Now, the expectation value of the exchange interaction between the carriers and the Mn d electrons (total ionic spin $S=\frac{5}{2}$) is given by[17]

$$\langle H_{\rm ex}\rangle_{m\mu}=-\alpha\sum_i|\phi(\mathbf{R}_i)|^2mS_{iz} -\frac{\beta}{3}\sum_{i,\lambda,\xi}F^*_{\lambda\mu}(\mathbf{R}_i)\langle\lambda|\mathbf{j}\cdot\mathbf{S}_i|\xi\rangle F_{\xi\mu}(\mathbf{R}_i), \tag{6}$$

where i labels the Mn ion sites and α (β) denotes the sp-d exchange parameter for an electron (hole). The effective exchange field acting on a Mn spin at $\mathbf{r}$ is thus

$$\mathbf{B}_{\rm eff}(\mathbf{r})=\frac{1}{g\mu_B}\left[\alpha m|\phi(\mathbf{r})|^2\hat{\mathbf{z}}+\frac{\beta}{3}\sum_{\lambda,\xi}F^*_{\lambda\mu}(\mathbf{r}) \times\langle\lambda|\mathbf{j}|\xi\rangle F_{\xi\mu}(\mathbf{r})\right]. \tag{7}$$

Note that the exchange field of the hole contains an angular dependence even if we neglect its transverse components. In order to restitute the spherical symmetry of our self-consistent problem we, therefore, average over the orientations $\mathbf{r}$ in Eq. (7). Then

$$B_{\rm eff}(r)=\frac{1}{g\mu_B}\left[\alpha m|\phi(r)|^2+\frac{\beta}{3}\mu\left(|f(r)|^2+\frac{1}{5}|g(r)|^2\right)\right] \tag{8}$$

along the mean-field axis z. Here,

$$f(r)\equiv\frac{1}{\sqrt{4\pi}}R_0(r),\quad g(r)\equiv\frac{1}{\sqrt{4\pi}}R_2(r) \tag{9}$$

so that

$$\int_0^a(|f(r)|^2+|g(r)|^2)4\pi r^2dr=1. \tag{10}$$

The magnetic free energy can be written as

$$G_{\rm mag}=-\int d\mathbf{r}\int_0^{B_{\rm eff}(\mathbf{r})}M(B)dB, \tag{11}$$

where $M(B)$ is the magnetization of the Mn spin system (assumed continuous). The total free energy of the e-h pair and the Mn magnetization cloud is

$$G=G_{\rm mag}+T_e+T_h+V_{\rm dir}+V_{\rm exch}, \tag{12}$$

where T_e (T_h) is the expectation value of the electron (hole) kinetic energy in the effective-mass approximation. $V_{\rm dir}$ ($V_{\rm exch}$) represents the direct (exchange) Coulomb interaction between the electron and the hole. The different terms are given below. We have

$$T_e=\int d\mathbf{r}\phi^*(r)\left[-\frac{\hbar^2}{2m_e}\left(\frac{d^2}{dr^2}+\frac{2}{r}\frac{d}{dr}\right)\right]\phi(r), \tag{13}$$

where m_e is the electron effective mass. The hole kinetic energy is given by[24]

$$\begin{aligned}T_h=&-\frac{\hbar^2}{2m_0}\gamma_1\Bigg[\int d\mathbf{r}f^*(r)\left\{\left(\frac{d^2}{dr^2}+\frac{2}{r}\frac{d}{dr}\right)f(r)\right.\\&\left.-\mu_{\rm BL}\left(\frac{d^2}{dr^2}+\frac{5}{r}\frac{d}{dr}+\frac{3}{r^2}\right)g(r)\right\}\\&+\int d\mathbf{r}g^*(r)\left\{-\mu_{\rm BL}\left(\frac{d^2}{dr^2}-\frac{1}{r}\frac{d}{dr}\right)f(r)\right.\\&\left.+\left(\frac{d^2}{dr^2}+\frac{2}{r}\frac{d}{dr}-\frac{6}{r^2}\right)g(r)\right\}\Bigg].\end{aligned} \tag{14}$$

Here m_0 is the free-electron mass. The Baldereschi-Lipari parameter $\mu_{\rm BL}\equiv(4\gamma_2+6\gamma_3)/(5\gamma_1)$, where γ_1, γ_2, and γ_3 are the Luttinger parameters. The e-h Coulomb interaction energy

$$V_{\rm dir}=-\frac{e^2}{\epsilon}\int d\mathbf{r}\int d\mathbf{r}'\frac{1}{r_>}|\phi(r)|^2(|f(r')|^2+|g(r')|^2), \tag{15}$$

where ϵ is the static dielectric constant and $r_>$ the greater of r and r'.

Starting from the effective e-h exchange Hamiltonian of the form $-\Delta\mathbf{s}\cdot\mathbf{j}\delta(\mathbf{r}_e-\mathbf{r}_h)$ we have the expectation value

$$V_{\rm exch}=-\Delta m\mu\int d\mathbf{r}|\phi(r)|^2(|f(r)|^2+|g(r)|^2). \tag{16}$$

After collecting all the terms in the total free energy G we apply the usual variational recipe for minimization:

$$\begin{gathered}\frac{\delta}{\delta\phi^*}(G-E_eN_e)=0,\quad\frac{\delta}{\delta f^*}(G-E_hN_h)=0,\\\frac{\delta}{\delta g^*}(G-E_hN_h)=0,\end{gathered} \tag{17}$$

where $N_{e,h}$ and $E_{e,h}$ represent the norms and the Lagrange multipliers, respectively. We thus obtain a system of three coupled Schrödinger equations

$$\begin{aligned}&-\frac{\hbar^2}{2m_e}\left(\frac{d^2}{dr^2}+\frac{2}{r}\frac{d}{dr}\right)\phi(r)-\left[\frac{\alpha m}{g\mu_B}M(B_{\rm eff}(r))\right.\\&\quad+\frac{e^2}{\epsilon}\int d\mathbf{r}'\frac{1}{r_>}\{|f(r')|^2+|g(r')|^2\}+\Delta m\mu\{|f(r)|^2\\&\quad\left.+|g(r)|^2\}\right]\phi(r)=E_e\phi(r),\end{aligned} \tag{18}$$

$$\begin{aligned}&-\frac{\hbar^2\gamma_1}{2m_0}\left(\frac{d^2}{dr^2}+\frac{2}{r}\frac{d}{dr}\right)f(r)-\left[\frac{\beta\mu}{3g\mu_B}M(B_{\rm eff}(r))\right.\\&\quad\left.+\frac{e^2}{\epsilon}\int d\mathbf{r}'\frac{1}{r_>}|\phi(r')|^2+\Delta m\mu|\phi(r)|^2\right]f(r)\\&\quad+\frac{\hbar^2\gamma_1}{2m_0}\mu_{\rm BL}\left(\frac{d^2}{dr^2}+\frac{5}{r}\frac{d}{dr}+\frac{3}{r^2}\right)g(r)=E_hf(r),\end{aligned} \tag{19}$$

$$\begin{aligned}&-\frac{\hbar^2\gamma_1}{2m_0}\left(\frac{d^2}{dr^2}+\frac{2}{r}\frac{d}{dr}-\frac{6}{r^2}\right)g(r)-\left[\frac{\beta\mu}{15g\mu_B}M(B_{\rm eff}(r))\right.\\&\quad\left.+\frac{e^2}{\epsilon}\int d\mathbf{r}'\frac{1}{r_>}|\phi(r')|^2+\Delta m\mu|\phi(r)|^2\right]g(r)\\&\quad+\frac{\hbar^2\gamma_1}{2m_0}\mu_{\rm BL}\left(\frac{d^2}{dr^2}-\frac{1}{r}\frac{d}{dr}\right)f(r)=E_hg(r).\end{aligned} \tag{20}$$

For the local magnetization functional, following Ref. 19, we shall use the experimental high-field magnetization curve[25]

$$M(H)=g\mu_BN_0x_{\rm eff}SB_S\left(\frac{Sg\mu_BH}{k(T+T_0)}\right)+\alpha_lH, \tag{21}$$

where B_S is the Brillouin function and $S=5/2$. N_0 is the number of cations per unit volume. The phenomenological parameters $x_{\rm eff}$ (reduced effective concentration of Mn) and T_0 account for the reduced single-ion contribution due to the antiferromagnetic Mn-Mn coupling, while the linear term with the coefficient α_l arises from the Mn cluster contributions. Recall that the effective field $B_{\rm eff}(r)$ is given by Eq. (8). Thus, even in the spherical approximation we are left with the formidable problem of solving three nonlinear coupled differential equations. Only some limiting cases can be discussed analytically. Note that the total polaron spin is

$$S_p=\frac{1}{g\mu_B}\int_0^a 4\pi r^2 dr M(B_{\rm eff}(r)) \tag{22}$$

and the polaron binding energy

$$E_p=\int_0^a 4\pi r^2 dr B_{\rm eff}(r) M(B_{\rm eff}(r)). \tag{23}$$

Clearly, the (hypothetical) complete saturation limit corresponds to $M_{\rm sat}=g\mu_B N_0 x(5/2)$ giving

$$E_p^{\rm sat}=N_0 x\tfrac{5}{2}(\alpha m+\tfrac{1}{3}\beta\mu\rho_p) \tag{24}$$

where

$$\rho_p\equiv\int_0^a 4\pi r^2 dr(|f(r)|^2+\tfrac{1}{5}|g(r)|^2). \tag{25}$$

In this limit, which would correspond to very small QD's, we can neglect the orbital contraction due to polaron formation. With the nonmagnetic QD hole wave functions[22] for $f(r)$ and $g(r)$ we can identify ρ_p as the Zeeman effect reduction factor ρ defined in Ref. 17 that depends only on the ratio of the light- and heavy-hole effective masses.

The Mn-Mn antiferromagnetic coupling makes it impossible to achieve complete saturation when $x\sim 0.1$. But partial saturation corresponding to the saturation of the Brillouin function in Eq. (21) can be realized in QD's of moderately small size $a\sim 15$ Å as $T\to 0$. In this regime

$$M(B_{\rm eff}(r))=g\mu_B N_0 x_{\rm eff}(5/2)+\alpha_l B_{\rm eff}(r) \tag{26}$$

giving

$$S_p=N_0 x_{\rm eff}(5/2)\frac{4\pi a^3}{3}+\frac{\alpha_l}{(g\mu_B)^2}\left(\alpha m+\frac{1}{3}\beta\mu\rho_p\right) \tag{27}$$

and

$$E_p=N_0 x_{\rm eff}(5/2)(\alpha m+\tfrac{1}{3}\beta\mu\rho_p)+\alpha_l\int_0^a 4\pi r^2 dr[B_{\rm eff}(r)]^2. \tag{28}$$

It is important to notice that, as $B_{\rm eff}(r)$ increases with decreasing r, near the center of small-size QD's the linear term in Eq. (26) has to be limited to the maximum value compatible with complete local saturation. However, this situation does not arise in moderately small QD's. Then, if we neglect the QD size dependence of the orbital contraction, it is easy to check that the integral in Eq. (28) is inversely proportional to the QD volume.

Let us now consider the high-temperature fluctuation regime realized in larger QD's, when the Brillouin function can be approximated by the linear term $\{B_S(x)\sim[(S+1)/S](x/3)\}$. Then

$$S_p=\left[\frac{N_0 x_{\rm eff}(35/12)}{k(T+T_0)}+\frac{\alpha_l}{(g\mu_B)^2}\right]\left(\alpha m+\frac{1}{3}\beta\mu\rho_p\right) \tag{29}$$

and

$$E_p=\left[\frac{N_0 x_{\rm eff}(35/12)}{k(T+T_0)}+\frac{\alpha_l}{(g\mu_B)^2}\right]\int_0^a 4\pi r^2 dr[\mu_B g B_{\rm eff}(r)]^2. \tag{30}$$

Thus, roughly speaking, at high T the total polaron spin is almost size independent and the polaronic binding inversely proportinal to the QD volume.

Note that the e-h exchange interaction has been found to yield a substantial singlet-triplet splitting in small QD's of CdSe (see Ref. 26). As $\alpha>0$ and $\beta<0$, the doubly degenerate mean-field polaron ground state is given by $m=\pm\frac{1}{2},\mu=\mp\frac{3}{2}$, with the electron spin aligned parallel to the average Mn spin direction and the hole spin antiparallel to it. This, of course, corresponds to the e-h singlet. We have verified that the triplet magnetic polaron, with the electron and hole spins parallel, has a much higher energy even in small-size QD's where the e-h exchange interaction partly compensates for the polaronic energy difference. Therefore, we focus our attention on the lowest-energy singlet magnetic polaron. Note, however, that the polaronic energy of this ground state would be slightly affected by the e-h exchange through orbital extension. It is estimated to be less than a percent in the smallest QD's considered. In view of the uncertainties concerning the exchange parameter Δ, we have chosen to drop this term altogether.

We finally solve the coupled equations [Eqs. (18)–(20)] for the MP ground state exactly through an iterative numerical procedure explained in the Appendix. The resulting self-consistent solution $\{\phi(r),f(r),g(r)\}$ shows an orbital contraction due to e-h Coulomb attraction and magnetic polaron formation. The polaron binding energy and total spin are calculated as functions of temperature for different values of the QD radius. In order to compute the polaron energy in the presence of an external magnetic field (B), we replace $B_{\rm eff}$ by $B+B_{\rm eff}$ in the equations above. The true polaron binding energy in B is then obtained after subtracting off the Zeeman shift of the e-h excitation energy: $E_Z=\frac{1}{2}(\alpha-\rho\beta)M(B)/(g\mu_B)$ from E_p given by Eq. (23).

Light-induced magnetization enhancement is studied in the superparamagnetic picture in the low-temperature and low-field limit. The equilibrium polaron magnetic moment is then

$$M_p=\frac{1}{3}(g\mu_B)^2 S_p^2\left(\frac{B}{kT}\right). \tag{31}$$

On the other hand, in the absence of polaron formation, the QD magnetic moment is given by $M_0=(4\pi a^3/3)M(B)$. Thus the low-field magnetization enhancement ratio $R\equiv M_p/M_0$ is

$$R=\frac{4}{35}\left(\frac{T+T_0}{T}\right)\frac{S_p^2}{N_{\rm eff}}(1-\delta), \tag{32}$$

where $N_{\rm eff}=N_0 x_{\rm eff}(4\pi a^3/3)$ and

$$\delta=\left(\frac{12}{35}\right)\frac{k(T+T_0)}{N_0 x_{\rm eff}(g\mu_B)^2}\alpha_l. \tag{33}$$

Numerical results are presented and discussed in the next section.

III. RESULTS AND DISCUSSION

Most of our numerical results correspond to nanocrystals of $Cd_{1-x}Mn_xTe$, because experimental high-field (up to 40

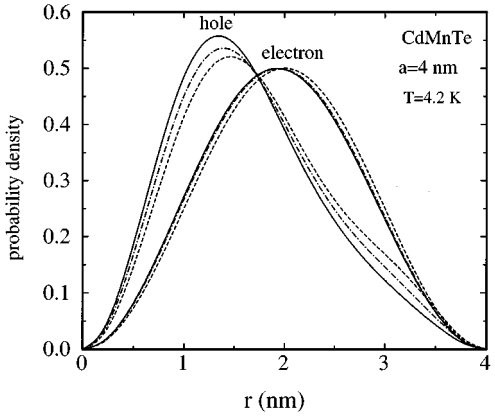

FIG. 1. Radial probability densities of the electron and hole (in units of nm^{-1}) are shown for a $Cd_{0.89}Mn_{0.11}Te$ quantum dot of radius $a=4$ nm. The dashed curves correspond to noninteracting confined particles; the dot-dashed ones result from the electron-hole Coulomb interaction. The solid curves represent the equilibrium magnetic polaron at $T=4.2$ K.

T) magnetization curves are available[25] for the bulk material. We choose $x=0.11$, which is close to the maximum of susceptibility, as a function of concentration. Then, $x_{\rm eff}=0.038$, $T_0=2.5$ K, and $\alpha_I=0.22\times10^{-4}$ erg/(G^2 cm^3). Also, we use the following CdTe parameters: $\epsilon=10$, $N_0=1.47\times10^{22}/\mathrm{cm}^3$, and $m_e=0.096m_0$. For the valence band Luttinger parameters, we use a recently determined set:[27] $\gamma_1=4.7$, $\gamma_2=1.45$, $\gamma_3=1.9$, giving $\mu_{\rm BL}=0.732$. Finally, the exchange parameters are $N_0\alpha=0.22$ eV and $N_0\beta=-0.88$ eV.[28]

Figure 1 illustrates the orbital contraction due to e-h Coulomb interaction and magnetic polaron formation. The radial probability density of the electron $(4\pi r^2|\phi(r)|^2)$ and that of the hole $(4\pi r^2[|f(r)|^2+|g(r)|^2])$ are plotted against r for a QD of radius $a=4$ nm. The dashed curves correspond to the noninteracting confined particles. The dot-dashed curves are obtained when the e-h Coulomb interaction is considered. Finally, the solid curves correspond to the equilibrium magnetic polaron at $T=4.2$ K. Clearly, the orbital contraction of the electron is much smaller than that of the hole, because of the smaller effective mass and weaker exchange coupling.

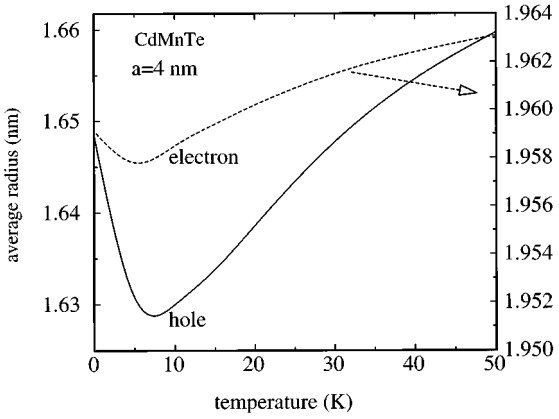

FIG. 2. The solid (dashed) curve shows the temperature dependence of the average radius of the hole (electron) in the magnetic polaron in a $Cd_{0.89}Mn_{0.11}Te$ quantum dot of radius $a=4$ nm.

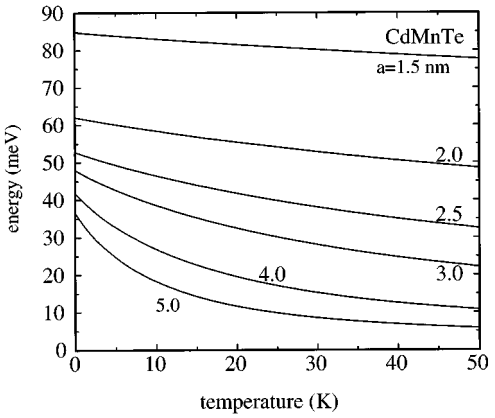

FIG. 3. Zero-field polaron binding energy (meV) vs temperature (K) in $Cd_{0.89}Mn_{0.11}Te$ quantum dots. Different curves correspond to the different values of a: 1.5, 2, 2.5, 3 , 4 , and 5 nm.

Note also that the e-h Coulomb interaction leads to a substantial orbital contraction, which tends to enhance the polaron binding energy and reduce the polaron spin. In Fig. 2, we present the average electron (r_e) and hole (r_h) radii of the magnetic polaron as functions of temperature. Note that $r_h(T)$ shows a well-defined minimum, which is related to the competition between the polaronic and localization energies.

Figure 3 shows the zero-field polaron binding energy E_p as a function of temperature for different values of the QD radius a. Clearly, E_p decreases with increasing QD radius. In small QD's ($a\leqslant2$ nm) the decrease of E_p vs T is relatively slow; here saturation is approached in the core region. In large QD's ($a\geqslant4$ nm) the decrease is faster and the fluctuation regime is approached at $T>30$ K, where $E_p\propto1/a^3$. The temperature dependence of the total polaron spin S_p, which is proportional to the spontaneous magnetic moment, is shown in Fig. 4 for the same values of a. As for the qualitative behavior, the $S_p(T)$ curves are rather similar to the $E_p(T)$ curves. They, however, show a faster initial decrease, and in the fluctuation regime S_p tends to a value that is independent of the QD size, in agreement with Eq. (29).

We show the dependence of the polaronic binding energy on the applied magnetic field in Figs. 5 and 6, for $a=$ 1.5

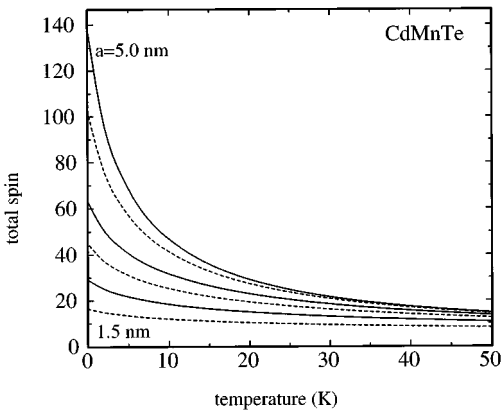

FIG. 4. Zero-field polaron spin vs temperature (K) in $Cd_{0.89}Mn_{0.11}Te$ quantum dots. Different curves correspond to the different values of a: 1.5, 2, 2.5, 3, 4, and 5 nm.

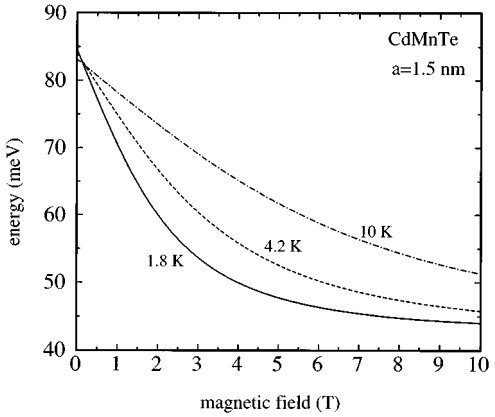

FIG. 5. Polaron binding energy (meV) vs magnetic field (tesla) in a $Cd_{0.89}Mn_{0.11}Te$ quantum dot of radius 1.5 nm at different temperatures: $T=1.8$, 4.2, and 10 K.

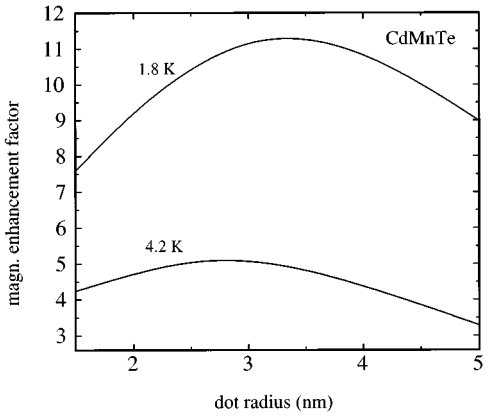

FIG. 7. Light-induced magnetization enhancement factor R plotted against the QD radius a (nm) at $T=1.8$ and 4.2 K for $Cd_{0.89}Mn_{0.11}Te$ quantum dots.

and 5.0 nm, respectively. In both figures three different temperatures are considered: $T=$ 1.8, 4.2, and 10 K. Let us recall that the Zeeman shift of the e-h creation energy has been subtracted from E_p in order to deduce the true polaron binding energy shown here. The decrease of polaron binding with increasing B is faster at lower temperatures. In small-size QD's (Fig. 5) there remains a substantial binding energy even at 10 T, because the polaronic effective field in the core region is much larger than B and can orient Mn spins further. On the other hand, in large dots (Fig. 6) the binding energy tends to decrease faster towards a small value.

Figure 7 presents the light-induced magnetization enhancement factor R defined in Eq. (32). In fact, it is the ratio of the magnetization due to polaron orientation in a small external field over that due to the Mn spins (in the absence of polaron formation). We plot R against a at $T=1.8$ and 4.2 K only. The superparamagnetic picture would probably break down at higher temperatures. The curve for $T=1.8$ K shows a rather well-defined maximum around $a=3$ nm. It is an indication of the optimum QD size for observing light-induced magnetization enhancement due to polaron formation suggested previously.[17]

It is interesting to note that the results presented above are quite sensitive to the values of the Luttinger parameters. For example, with the Lawaetz values for CdTe, $\gamma_1=5.29$, $\gamma_2=1.89$, $\gamma_3=2.46$, giving $\mu=0.844$, we obtain $E_p(T=0)=$ 74.2 and 33.2 meV, for $a=$ 1.5 and 5.0 nm, respectively. These energy values are smaller than the corresponding ones in Fig. 3, obtained from the Luttinger parameters of Ref. 27.

Previously,[29] for numerical calculations, we resorted to the usual approximation of the MP theory for the hole, which neglects the mixing of the light- and heavy-hole bands. It amounted to formally setting $g(r)=0$ in Eqs. (18)–(20), thus reducing the problem to a set of two coupled equations. A comparison of the results (an example can be seen in Fig. 8) shows that the simplifying approximation is utterly inadequate. In particular, it yields a larger hole radius, leading to a smaller polaron binding energy; the quantitative differences with the exact solution presented here are indeed large.

While Figs. 1–7 all correspond to $Cd_{0.89}Mn_{0.11}Te$, Fig. 8 corresponds to $Cd_{0.9}Mn_{0.1}Se$. It shows the polaron binding energy as a function of applied field in a QD of radius $a=8$ nm at $T=4.2$ K. The parameters used for calculating the theoretical curves are as follows: $\epsilon=8.9$, $m_e=0.15m_0$,

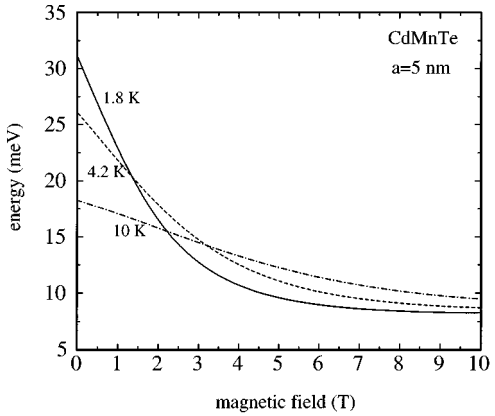

FIG. 6. Polaron binding energy (meV) vs magnetic field (tesla) in a $Cd_{0.89}Mn_{0.11}Te$ quantum dot of radius 5 nm at different temperatures: $T=1.8$, 4.2, and 10 K.

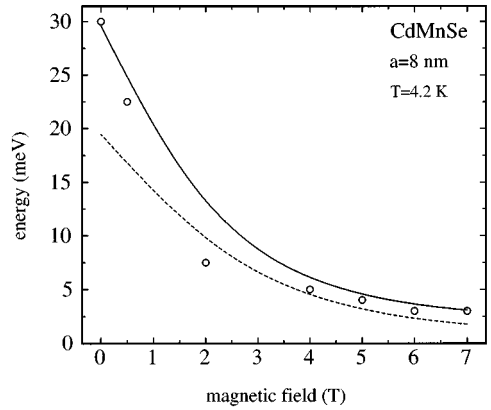

FIG. 8. Polaron binding energy (meV) vs magnetic field (tesla) in a $Cd_{0.9}Mn_{0.1}Se$ quantum dot of radius 8 nm at $T=4.2$ K. The solid curve is the result of the present calculation; the dashed one is from Ref. 29 (simplified model). The circles represent experimental values deduced from photoluminescence Stokes shift data (Ref. 16) for $x=0.12$ and *average* radius 8 nm.

and $N_0=1.77\times10^{22}/\mathrm{cm}^3$. Using $m_\perp^A=0.45m_0$ and $m_\parallel^A=1.15m_0$ from Ref. 30, we obtain $\gamma_1=1.77$ and $\mu_{\mathrm{BL}}=0.509$. Also, $N_0\alpha=0.26$ eV and $N_0\beta=-1.11$ eV.[31] From the experimental magnetization data up to 8 T (Ref. 31). we have $x_{\mathrm{eff}}=0.039$ and $T_0=2.3$ K. In view of the closeness of these two values to those for $Cd_{0.9}Mn_{0.1}Te$ and in the absence of high-field magnetization data in $Cd_{0.9}Mn_{0.1}Se$, we have assumed the same value of α_I for the linear coefficient in Eq. (21). Anyway, for such a large value of a, the contribution of the linear term is small. The solid curve in Fig. 8 results from the exact solution presented here, while the dashed one is from Ref. 29 and is based on the simplifying approximation explained in the preceding paragraph. In addition to the theoretical curves, Fig. 8 also shows the experimental[16] photoluminescence Stokes shift values after subtracting 50 meV for the exciton localization energy, following the authors of Ref. 16. It is satisfying to see that the exact solution yields a significantly better agreement with experiment. Note that no adjustable parameter has been used. One should, however, keep in mind that here $a=80$ Å is larger than the CdSe exciton Bohr radius $a_B=56$ Å and we are apparently beyond the strong (independent particle) confinement regime assumed throughout this paper. Let us also point out that the application of our model to the case of the wurtzite crystal $Cd_{1-x}Mn_xSe$ assumes that the splitting between A and B hole bands is smaller than the hole confinement energy, and the magnetic field is parallel to the c axis.[18]

IV. CONCLUDING REMARKS

We have presented a self-consistent mean-field model for the magnetic polaron associated with an electron-hole pair in a semimagnetic semiconductor nanocrystal. The effective Schrödinger equations are derived for a fourfold degenerate valence band in the spherical approximation. An experimental high-field magnetization curve in the bulk is used to model the local response of Mn spins to the exchange field of the confined carriers. Numerical results are presented mostly for $Cd_{0.9}Mn_{0.1}Te$ nanocrystals in the radius range 15–50 Å at temperatures up to 50 K and fields up to 10 T. The polaron binding energy decreases with increasing size, temperature, or magnetic field. The spontaneous magnetic moment of the polaron also decreases with increasing temperature. Small QD's show saturating polaron behavior at low temperature, while large ones approach the fluctuation regime at high temperature. Light-induced magnetization enhancement due to polaron formation is predicted to be maximum around $a=30$ Å at $T=1.8$ K. No experimental data are, however, available in $Cd_{1-x}Mn_xTe$ nanocrystals. Yanata *et al.*[16] reported experimental evidence of localized exciton magnetic polaron in $Cd_{0.9}Mn_{0.1}Se$ nanocrystals of average radius 80 Å. Our theoretical curve for polaron binding energy *versus* applied field shows a good agreement with the experimental values derived from the photoluminescence Stokes shift under selective excitation. Hopefully, the present work would stimulate more systematic experimental studies of DMS nanocrystals.

APPENDIX: NUMERICAL METHOD

Here we present our method for an iterative numerical solution of the three coupled effective Schrödinger equations [Eqs. (18)–(20)]. Neglecting the e-h exchange term and setting $\mu=\mp3/2$, $m=\pm1/2$ for the MP ground state, the equations can be rewritten as

$$-\frac{\hbar^2}{2m_e}\Delta_r\phi(r)+U^e(r)\phi(r)=E_e\phi(r), \tag{A1}$$

$$-\frac{\hbar^2\gamma_1}{2m_0}\left[\Delta_r f(r)-\mu_{\mathrm{BL}}\left(\frac{d^2}{dr^2}+\frac{5}{r}\frac{d}{dr}+\frac{3}{r^2}\right)g(r)\right]+U^f(r)f(r)=E_h f(r), \tag{A2}$$

$$-\frac{\hbar^2\gamma_1}{2m_0}\left[\left(\Delta_r-\frac{6}{r^2}\right)g(r)-\mu_{\mathrm{BL}}\left(\frac{d^2}{dr^2}-\frac{1}{r}\frac{d}{dr}\right)f(r)\right]+U^g(r)g(r)=E_h g(r), \tag{A3}$$

with $\Delta_r\equiv d^2/dr^2+(2/r)(d/dr)$. Each effective potential $U^i(r)\equiv U_C^i(r)+U_M^i(r)$ is a sum of the Coulomb and magnetic contributions given by

$$U_C^e(r)=-(e^2/\epsilon)\int d\mathbf{r}'[|f(r')|^2+|g(r')|^2]/r_>,$$

$$U_M^e(r)=-(\alpha/2g\mu_B)M(B_{\mathrm{eff}}(r)),$$

$$U_C^f(r)=U_C^g(r)=-(e^2/\epsilon)\int d\mathbf{r}'|\phi(r')|^2/r_>,$$

$$U_M^f(r)=-(|\beta|/2g\mu_B)M(B_{\mathrm{eff}}(r)),U_M^g(r)=U_M^f(r)/5.$$

The effective exchange field is

$$B_{\mathrm{eff}}(r)=\frac{1}{2g\mu_B}[\alpha|\phi(r)|^2+|\beta|(|f(r)|^2+\tfrac{1}{5}|g(r)|^2)].$$

Now, in order to solve Eqs. (A1)–(A3), we write the envelope functions in terms of the sine series:[21]

$$\phi(r)=\frac{1}{\sqrt{2\pi a}}\left(\frac{1}{r}\right)\sum_{n=1}^{N}\phi_n\sin\left(\frac{n\pi r}{a}\right) \tag{A4}$$

and similarly for $f(r)$ and $g(r)$ with the expansion coefficients f_n and g_n, respectively. The functions satisfy the boundary condition at $r=a$ and their normalization corresponds to $\Sigma|\phi_n|^2=1$ and $\Sigma(|f_n|^2+|g_n|^2)=1$. The number N is eventually chosen large enough to achieve convergence. Equations (A1)–(A3) are thus reduced to the (formally) linear equations

$$m^2\phi_m+\sum u_{mn}^e\phi_n=(E_e/E_{e0})\phi_m, \tag{A5}$$

$$m^2 f_m+\sum u_{mn}^f f_n-\mu_{\mathrm{BL}}m^2 g_m+(3\mu_{\mathrm{BL}}/\pi)\sum nV_{mn}^+ g_n=(E_h/E_{h0})f_m, \tag{A6}$$

$$m^2 g_m + \sum [u^g_{mn} + (6/\pi)(mV^-_{mn} + nV^+_{mn})]g_n - \mu_{\rm BL} m^2 f_m$$

$$+ (3\mu_{\rm BL}/\pi) m \sum V^-_{mn} f_n = (E_h/E_{h0}) g_m . \qquad \text{(A7)}$$

Here $E_{e0} = \hbar^2\pi^2/2m_e a^2$, $E_{h0} = \gamma_1 \hbar^2 \pi^2/2m_0 a^2$, $u^e_{mn} = U^e_{mn}/E_{e0}$, $u^f_{mn} = U^f_{mn}/E_{h0}$, $u^g_{mn} = U^g_{mn}/E_{h0}$, with

$$U^i_{mn} \equiv (2/a) \int_0^a \sin(m\pi r/a) U^i(r) \sin(n\pi r/a) dr, \quad \text{(A8)}$$

and $V^{\pm}_{mn} = \mathrm{Si}[(m+n)\pi] \pm \mathrm{Si}[(m-n)\pi]$, where $\mathrm{Si}(x)$ is the usual sine integral. We see that the problem has been reduced to the diagonalization of one $N \times N$ matrix and one $2N \times 2N$ matrix. In our applications, $N = 30$ is found sufficient to assure a good convergence of the eigenvalues. The self-consistent potential problem is solved iteratively, starting from the free particle case: $U^i(r) = 0$. At each step of iteration the potentials are calculated from the ground-state vectors of the preceding diagonalization. The matrix elements of the Coulomb potential can be expressed in terms of the Si functions and those of the exchange field calculated through fast Fourier transform routines. Depending on the MP binding energy, only 5 to 15 iterations are necessary to obtain a convergence better than 10^{-4}. The practically exact solution $\{\phi(r), f(r), g(r)\}$ thus obtained is used to calculate the MP equilibrium properties: orbital size, binding energy (E_p), and total spin (S_p).

[1] For a review see Y. Wang and N. Herron, J. Phys. Chem. **95**, 525 (1991).

[2] C. B. Murray, D. J. Norris, and M. G. Bawendi, J. Am. Chem. Soc. **115**, 8706 (1993); D. J. Norris, A. Sacra, C. B. Murray, and M. G. Bawendi, Phys. Rev. Lett. **72**, 2612 (1994).

[3] For a recent review see C. Benoit à la Guillaume, in *Proceedings of the 22nd International Conference on the Physics of Semiconductors, Vancouver, 1994*, edited by D. L. Lockwood (World Scientific, Singapore, 1995), p. 2585.

[4] P. A. Wolff, in *Diluted Magnetic Semiconductors*, edited by J. K. Furdyna and J. Kossut, Semiconductors and Semimetals Vol. 25 (Academic, New York, 1988), Chap. 10.

[5] A. Golnik, J. Ginter, and J. A. Gaj, J. Phys. C **16**, 6073 (1983); H. Akinaga, K. Takita, S. Sasaki, S. Takeyama, N. Miura, T. Nakayama, F. Minami, and K. Inoue, Phys. Rev. B **46**, 13 136 (1992); G. Mackh, W. Ossau, D. R. Yakovlev, A. Waag, G. Landwehr, R. Hellmann, and E. O. Göbel, *ibid.* **49**, 10 248 (1994).

[6] D. R. Yakovlev, W. Ossau, G. Landwehr, R. N. Bicknell-Tassius, A. Waag, S. Schmeusser, and I. N. Uraltsev, Solid State Commun. **82**, 29 (1992); G. Mackh, W. Ossau, D. R. Yakovlev, R. Hellmann, E. O. Göbel, T. Wojtowicz, G. Karczewski, J. Kossut, and G. Landwehr, in *Proceedings of the International Conference on Semiconductor Heteroepitaxy, Montpellier, 1995*, edited by B. Gil and R.-L. Aulombard (World Scientific, Singapore, 1995), p. 210.

[7] Tran Hong Nhung and R. Planel, Physica B **117-118**, 488 (1983).

[8] A. K. Bhattacharjee, R. Planel, and C. Benoit à la Guillaume, in *Proceedings of the 17th International Conference on the Physics of Semiconductors, San Francisco, 1984*, edited by J. D. Chadi and W. A. Harrison (Springer-Verlag, New York, 1985), p. 1431.

[9] Tran Hong Nhung, R. Planel, C. Benoit à la Guillaume, and A. K. Bhattacharjee, Phys. Rev. B **31**, 2388 (1985).

[10] J. Warnock and P. A. Wolff, Phys. Rev. B **31**, 6579 (1985).

[11] D. Heiman, J. Warnock, P. A. Wolff, R. Kershaw, D. Ridgley, K. Dwight, and A. Wold, Solid State Commun. **52**, 909 (1984).

[12] D. Scalbert, M. Nawrocki, C. Benoit à la Guillaume, and J. Cernogora, Phys. Rev. B **33**, 4418 (1986).

[13] A. K. Bhattacharjee, Phys. Rev. B **35**, 9108 (1987).

[14] Y. Wang, N. Herron, K. Moller, and T. Bein, Solid State Commun. **77**, 33 (1991).

[15] R. N. Bhargava, D. Gallagher, X. Hong, and A. Nurmikko, Phys. Rev. Lett. **72**, 416 (1994).

[16] K. Yanata, K. Suzuki, and Y. Oka, J. Appl. Phys. **73**, 4595 (1993); K. Yanata and Y. Oka, Jpn. J. Appl. Phys. **34**, Suppl. 34-1, 164 (1995).

[17] A. K. Bhattacharjee, Phys. Rev. B **51**, 9912 (1995).

[18] A. K. Bhattacharjee, in *Proceedings of the International Conference on Semiconductor Heteroepitaxy, Montpellier, 1995*, edited by B. Gil and R.-L. Aulombard (World Scientific, Singapore, 1995), p. 179.

[19] L. R. Ram-Mohan and P. A. Wolff, Phys. Rev. B **38**, 1330 (1988).

[20] C. Benoit à la Guillaume, Phys. Status Solidi B **175**, 369 (1993); C. Benoit à la Guillaume, Yu. G. Semenov, and M. Combescot, Phys. Rev. B **51**, 14 124 (1995).

[21] J.-B. Xia, Phys. Rev. B **40**, 8500 (1989).

[22] Al. L. Efros, Phys. Rev. B **46**, 7448 (1992).

[23] T. Richard, P. Lefebvre, H. Mathieu, and J. Allègre, Phys. Rev. B **53**, 7287 (1996).

[24] A. Baldereschi and N. O. Lipari, Phys. Rev. B **8**, 2697 (1973).

[25] D. Heiman, E. D. Isaacs, P. Becla, and S. Foner, Phys. Rev. B **35**, 3307 (1987).

[26] M. Nirmal, D. J. Norris, M. Kuno, M. G. Bawendi, Al. L. Efros, and M. Rosen, Phys. Rev. Lett. **75**, 3728 (1995); M. Chamarro, C. Gourdon, P. Lavallard, O. Lublinskaya, and Al. L. Ekimov, Phys. Rev. B **53**, 1 (1996).

[27] Le Si Dang (unpublished): $\gamma_1 = 4.7 \pm 0.3p$, $\gamma_2 = 1.45 \pm 0.15p$, and $\gamma_3 = 1.9 \pm 0.2p$, where $0 \leqslant p \leqslant 1$.

[28] J. A. Gaj, R. Planel, and G. Fishman, Solid State Commun. **29**, 435 (1979).

[29] A. K. Bhattacharjee and C. Benoit à la Guillaume, in *Proceedings of the 23rd International Conference on the Physics of Semiconductors, Berlin, 1996*, edited by M. Scheffler and R. Zimmermann (World Scientific, Singapore, 1996), p. 1469.

[30] *Physics of Group IV Elements and III-V Compounds*, edited by O. Madelung, M. Schulz, and H. Weiss, Landolt-Börnstein, New Series, Group III, Vol. 17, Pt. A (Springer-Verlag, Berlin, 1982).

[31] R. L. Aggarwal, S. N. Jasperson, J. Stankiewicz, Y. Shapira, S. Foner, B. Khazai, and A. Wold, Phys. Rev. B **28**, 6907 (1983).